Microstructure of Melt-Miscible, Semicrystalline Polymer Blends

S. Talibuddin, L. Wu, and J. Runt*

Department of Materials Science and Engineering, The Pennsylvania State University, University Park, Pennsylvania 16802

J. S. Lin

Oak Ridge National Laboratory, Oak Ridge, Tennessee 37831

Received April 5, 1996; Revised Manuscript Received August 12, 1996[⊗]

ABSTRACT: A combination of small-angle X-ray scattering and optical microscopy was used to investigate the influence of diluent mobility and polymer−polymer interactions on diluent segregation in a series of "model" melt-miscible poly(ethylene oxide) (PEO) blends. The amorphous polymeric diluents were selected with regard to their glass transition temperatures relative to the crystallization temperature and the strength of their interactions with PEO. Segregation of the weakly interacting amorphous polymers was found to be largely dependent on their glass transition temperatures: the high-T_g diluent was found to reside exclusively in interlamellar regions whereas the low-T_g diluent was excluded at least partially into interfibrillar regions. The introduction of strong intermolecular interactions between the crystallizable and amorphous components resulted in significantly reduced crystal growth rates and promoted diluent segregation over greater length scales, regardless of diluent mobility at the crystallization temperature. Thus, for the systems under consideration here, the study shows that although diluent mobility contributes to diluent segregation, the growth of the PEO crystals, and the factors that influence the growth rate, dominate the length scale of diluent segregation.

I. Introduction

The analysis of the morphology of crystalline polymer blends has gained significant momentum over the years. Much attention has focused on the rich and varied microstructures that result from the crystallization of melt-miscible, semicrystalline/amorphous blends (e.g. refs 1−13). One of the important considerations in this case is the location of the amorphous polymeric diluent in the microstructure. The diluent molecules can reside in interspherulitic regions, interfibrillar regions (i.e. between the fibrils or lamellar stacks), interlamellar regions (between lamellar crystals), or some combination of these, yielding different microstructures, which in turn give rise to different material properties. It is important, therefore, to determine the factors that influence the extent of diluent segregation. It is also interesting to note that the disposition of the amorphous polymer in the final microstructure may result in multiple locations for the amorphous diluent, leading naturally to multiple T_g-like transitions (even in the absence of a relaxation associated with the crystal−amorphous interphases [see, for example, refs 4 and 14]), although the polymers themselves are miscible at this temperature.[15−17]

Microstructures of a range of melt-miscible, crystalline blends have been documented, some where the diluent polymer is exclusively interlamellar[1,2,6,11,12] and others where it is excluded, at least partially, into interfibrillar and/or interspherulitic regions.[7−10,13,15−17] What controls placement of the amorphous polymer in the microstructure of such melt-miscible systems? From the point of view of interlamellar incorporation, the diameter of gyration of the diluent polymer is often comparable to or greater than the separation between crystalline lamellae, particularly at high crystalline polymer concentrations.[6] Confinement of the diluent would therefore lead to an entropic driving force for escape from the interlamellar zones. In competition with this, it has been proposed that the favorable intermolecular interactions gained by mixing the diluent with the amorphous portion of the crystalline polymer will promote interlamellar incorporation.

From a review of the publications cited above (most are for relatively weakly interacting mixtures), it is generally found that the amorphous polymer resides in interlamellar regions when its glass transition temperature (T_g) is high compared to the crystallization temperature (T_c), whereas when its T_g is low relative to T_c at least some of the amorphous polymer is located outside of the interlamellar regions. A case in point is the poly(vinylidene fluoride) and poly(methyl methacrylate) (PMMA) blend system for which completely interlamellar[2,4] as well as extralamellar[13] placement of PMMA is observed at different T_cs. Thus mobility of the amorphous polymer, which is determined by its T_g and by the mixed phase environment at and away from the crystal growth front, appears to be one factor that plays an important role in diluent segregation. The role of the crystal growth rate is also expected to be important.[17,18]

Thus far, however, there have been no studies that specifically address the effects of diluent T_g and intermolecular interactions on crystalline blend microstructures. With this purpose in mind, we designed four "model" melt-miscible, semicrystalline/amorphous polymer blends and investigated the microstructure and crystallization kinetics. This paper deals primarily with the microstructure as revealed by small-angle X-ray scattering (SAXS), with a mild foray into growth kinetics studied via cross-polarized optical microscopy. A more detailed discussion of the latter will be published separately.

II. Experimental Section

Materials. Poly(ethylene oxide) (PEO) was used as the crystalline component in each model blend system while the

* To whom correspondence should be addressed.

[⊗] Abstract published in *Advance ACS Abstracts,* October 15, 1996.

S0024-9297(96)00508-6 CCC: $12.00 © 1996 American Chemical Society

Table 1. Volume Fraction Crystallinities of PEO Blends Crystallized at T_c = 45 °C As Determined via DSC

wt % diluent	PVAc	PMMA	EMAA55	SHS50
10	0.72	0.68	0.69	0.64
15		0.65	0.69	0.60
20	0.66	0.59	0.63	0.54
25	0.61	0.55		
30	0.57	0.50		
40	0.48	0.41		

melt-miscible amorphous polymers were selected with regard to their T_gs vis-á-vis the crystallization temperature and the strength of their interactions with PEO. PMMA and poly(vinyl acetate) (PVAc) represent "weakly interacting" high-T_g and low-T_g diluents (T_g = 113 and 31 °C, respectively). Both PMMA and PVAc are reported to be completely miscible with PEO in the melt.[5,6,19,20] Using small-angle neutron scattering and the random phase approximation, Ito and co-workers[21] have determined effective χ values on the order of -10^{-3} for PEO/PMMA blends containing both protonated and deuterated PMMA; thus PEO/PMMA can be regarded as a relatively weakly interacting mixture. Interactions between PEO and PVAc are also characterized as relatively weak.[22]

Two random copolymers, one composed of ethylene and methacrylic acid (containing 55% by weight acid units [EMAA55]), and another of 50 wt % styrene and *p*-hydroxystyrene [SHS50] were chosen as corresponding "strongly interacting" low-T_g and high-T_g diluents (T_g = 36 and 150 °C, respectively). DSC analysis performed previously[23] on quenched PEO/EMAA55 and PEO/SHS50 blends has yielded single composition-dependent glass transition temperatures, which are characteristic of miscible systems. Fourier transform infrared studies on PEO/EMAA55 blends have revealed strong hydrogen bonds between the two components.[24] While comparable spectroscopic studies have not been performed on PEO/SHS50 blends, infrared spectroscopic analysis of binary blends of PEO with poly(hydroxystyrene)[25] and a 55/45 styrene-*co*-hydroxystyrene copolymer[26] clearly indicate the presence of intermolecular hydrogen bonds in these systems.

PEO of viscosity-average molecular weight 1.44×10^5 was purchased from Polysciences and PMMA ($\bar{M}_w = 6.4 \times 10^4$, $\bar{M}_w/\bar{M}_n = 4.4$) and PVAc ($\bar{M}_w = 1.3 \times 10^5$, $\bar{M}_w/\bar{M}_n = 3.1$) from Aldrich. EMAA55 ($\bar{M}_w = 2.56 \times 10^4$, $\bar{M}_w/\bar{M}_n = 2.6$) and SHS50 ($\bar{M}_w = 9.95 \times 10^4$, $\bar{M}_w/\bar{M}_n = 2.8$) were supplied, respectively, by du Pont[27] and Hoechst Celanese. Average molecular weights presented for the amorphous polymers are the polystyrene-equivalent values as determined by gel permeation chromatography.

Glass transition temperatures of the amorphous polymers and bulk crystallinities of isothermally crystallized neat PEO and PEO blends were measured using a TA Instruments DSC 2910 differential scanning calorimeter. At each composition, a bulk crystallinitiy, based on a perfect heat of fusion ($\Delta H_f°$) of 203 J/g for PEO,[28] was determined by averaging results from three melting endotherms. These values are presented in Table 1. Typical uncertainties in the volume fraction crystallinities are estimated to be on the order of ±0.02.

Electron densities of PVAc, PMMA, and 100% crystalline and 100% amorphous PEO were calculated from their mass densities published in the literature.[28,29] These are 0.636 (ρ = 1.19 g/cm^3), 0.642 (ρ = 1.19 g/cm^3), 0.676 (ρ = 1.24 g/cm^3), and 0.612 (ρ = 1.12 g/cm^3) mol of electrons/cm^3, respectively. Approximately 2 g each of EMAA55 and SHS50 was compression-molded into void-free disks of fixed dimensions. Weight and volume measurements were then performed on the disks to yield the mass densities of the two copolymers. From these, the electron densities were computed as 0.528 (ρ = 0.958 g/cm^3) and 0.573 (ρ = 1.07 g/cm^3) mol of electrons/cm^3, respectively. These values are in good agreement with those determined using a group contribution approach, described in ref 22.

The electron and mass densities were used to compute bulk crystallinities (ϕ_c) and electron densities (η) for the case of all-interlamellar placement of the diluent, by employing the following relations:

$$\phi_c = (x_i x_c/\rho_c)/[(x_i x_c/\rho_c) + \{x_i(1 - x_c)\rho_a\} + (1 - x_i)/\rho_d] \quad (1)$$

(volume fractions of amorphous PEO, ϕ_a, and diluent polymer, ϕ_d, are obtained in a similar fashion) and

$$\eta = \phi_a\eta_a + \phi_d\eta_d \quad (2)$$

where x_i is the weight fraction of PEO in the blend; x_c is the ratio of crystalline PEO to overall PEO content in the blend as determined by DSC; ρ_c, ρ_a, and ρ_d are the respective mass densities of crystalline neat PEO, amorphous neat PEO, and amorphous diluent; and η_a and η_d are the amorphous neat PEO and amorphous diluent electron densities, respectively.

Sample Preparation. For each PEO/amorphous polymer system, a series of blend compositions was prepared by casting 2 wt % solutions in a suitable solvent: $CHCl_3$ for PEO/PMMA and PEO/PVAc, and 50/50 THF/CH_2Cl_2 for PEO/EMAA55 and PEO/SHS50. The resulting films were dried in air at room temperature for 48 h and then under vacuum at 90 °C for 6 h to ensure complete solvent removal. The dried films were pressed in a Carver hydraulic press at 69 MPa and 100 °C for 2 min and then rapidly cooled in air to room temperature. Neat PEO films were prepared by melt-pressing the powdery polymer under similar conditions. Films were then cut into thin strips and compression molded into 2 mm × 26 mm disks at 69 MPa and 100 °C to form samples for SAXS. Each sample was crystallized isothermally by melting at 100 °C in a Mettler FP82 hot stage for 10 min to erase thermal history, followed by immediate transfer to the press which was maintained at a crystallization temperature of 45 °C (neat PEO was additionally crystallized at T_c = 50 °C). The sample was held in the press at 69 MPa for a length of time determined to be in excess of that to ensure complete crystallization (6 and 24 h for neat PEO at T_c = 45 and 50 °C, respectively; 12−24 h for PEO/PVAc and PEO/PMMA; 48−96 h for PEO/EMAA55 and PEO/SHS50), removed, and allowed to cool to room temperature.

Samples for optical microscopy were prepared by casting the polymer solutions on glass slides followed by drying in air and vacuum as described above. Neat PEO was cast from a 2% chloroform solution.

Small-Angle X-ray Scattering. SAXS experiments were performed on the Oak Ridge National Laboratory 10 m pinhole collimated SAXS camera[30] using Cu Kα radiation (λ = 0.154 nm) and a 20 × 20 cm^2 position-sensitive area detector with ca. 3 mm cells. Scattered intensities were stored in a 64 × 64 array. Corrections were made for instrumentation background and detector efficiency with a ^{55}Fe radioactive standard on a cell-by-cell basis. Each specimen was measured at sample-to-detector distances of 2.119 and 5.119 m to extract data at high and low scattering angles, respectively. The data were azimuthally averaged in the respective high and low q ranges, $0.104 < q < 2.645$ nm^{-1} and $0.041 < q < 1.086$ nm^{-1}. Here, q is the scattering vector, defined as $(4\pi/\lambda)\sin(\theta/2)$, where θ is the scattering angle and λ is the X-ray wavelength. The data were converted to an absolute differential cross-section (cm^{-1} units) by means of precalibrated secondary standards[31]: a high-density polyethylene secondary standard, PES-3, was used for the low-q data and a vitreous carbon standard was employed for the high-q data.

For each sample, high-q data were suitably appended to the low-q data, and the scattered intensities were corrected for electronic noise. Intensities were truncated at $q \approx 0.078$ nm^{-1} as scatter from the beam stop was observed at lower angles. Corrections for thermal density fluctuations[32,33] were made by evaluating the slope of an Iq^4 vs q^4 plot at the "high-q" end ($1 < q < 2$ nm^{-1}) and subtracting it from the overall I vs q data. Peak maxima from Lorentz-corrected intensities (Iq^2 vs q) were employed to compute long periods as per Bragg's law, $L_{lor} = 2\pi/q$.

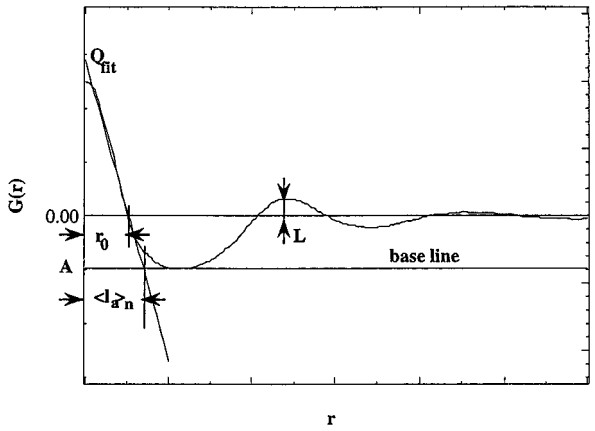

Figure 1. Typical one-dimensional correlation function and associated parameters for a semicrystalline polymer with $w_c > 0.5$.

The I vs q data were linearly extrapolated to $q = 0$ from $q \approx 0.078$ nm^{-1} to facilitate calculation of the one-dimensional correlation function:[34]

$$G(r) = (1/2\pi^2)\int q^2 I(q) \cos(qr)\, dq \tag{3}$$

where r is the correlation distance.

The generation of $G(r)$ customarily calls for extrapolation to large q values, which is achieved by the application of Porod's law for diffuse phase boundaries[34,35] to higher scattering vectors. However, if the diffuse interphase is much smaller than the average crystal thickness,[6,34] the ordinate of a linear fit to the self-correlation portion of the correlation function (constructed without extrapolation to large q) gives the invariant for a "pseudo-two phase" model, i.e., alternating crystal and amorphous layers with negligible interphase thickness. The application of Porod's law ($\ln Iq^4$ vs q^2) to our systems yielded transition zone thicknesses, $E = (12 \times |\text{slope}|)^{0.5}$, of ca. 1.5−2.5 nm. Since PEO lamellae possess thicknesses of nearly 20 nm at the crystallization temperatures used here, we assumed a negligible interphase and generated correlation functions without extrapolation to high q values. The pseudo-two phase model was applied to the correlation functions of neat PEO and the blends to extract the experimental invariant, Q_{fit}. Figure 1 depicts a schematic of the general shape of a one-dimensional correlation function for a semicrystalline polymer. The various parameters are defined as follows:[36]

$$Q_{fit} = v_s w_c (1 - w_c)\Delta\eta_l^2 \tag{4}$$

where w_c is the linear crystallinity (given by the ratio of the average lamellar thickness, $\langle l_c \rangle$, to the average long period, $\langle L \rangle$), v_s represents the volume fraction of lamellar stacks (given by the ratio of the bulk crystallinity, ϕ_c, to the linear crystallinity, w_c) and $\Delta\eta_l$ is the linear electron density difference, defined as $\Delta\eta_l = \eta_c - \eta_a$, where η_c and η_a are the electron densities of the crystal and amorphous layers, respectively. In the case of total interlamellar incorporation of uncrystallized material, the linear crystallinity and electron density difference, w_c and $\Delta\eta_l$, are replaced by their respective *bulk* values, ϕ_c and $\Delta\eta$, and the invariant reduces to[35]

$$Q_{int} = \phi_c(1 - \phi_c)\Delta\eta^2 \tag{5}$$

Here, $\Delta\eta = \eta_c - \eta$, where η is the electron density of the amorphous layer when all of the amorphous diluent lies within the interlamellar regions. Thus, one can calculate the "all-interlamellar" two-phase invariant, Q_{int}. Comparison with Q_{fit} indicates the extent of diluent inclusion in the interlamellar regions.

The average long period is given by

$$\langle L \rangle_n = \Delta\eta_l^2/(dG/dr)_{fit} \tag{6}$$

where $(dG/dr)_{fit}$ is the slope of the linear fit to the self-correlation portion of $G(r)$. For $w_c > 0.5$, the intersection of the linear fit with $G(r) = 0$ is

$$r_0 = \langle l_c \rangle_n (1 - w_c) = \langle l_a \rangle_n w_c \tag{7}$$

and the magnitude of the "baseline"[34] is defined as

$$A = Q_{fit}(1 - w_c)/w_c \tag{8}$$

For $w_c < 0.5$, w_c is replaced by $(1 - w_c)$ in the above equations.

Q_{fit}, $(dG/dr)_{fit}$ and r_0 are obtained directly from the fit to the self-correlation portion of $G(r)$. The numerical value of one additional parameter is needed to permit quantitative analysis of the lamellar microstructure using eqs 4−8. The magnitude of the baseline, A, or the average long period, L, is generally employed for this purpose. For $w_c < 0.3$ or $w_c > 0.7$, the baseline may coincide with the first minimum of the correlation function and can be used to solve for microstructural parameters, provided the lamellar stacks are "infinite". The occurrence of finite lamellar stacks (due to the presence of interfibrillar material) is believed to "damp" the correlation function,[37] rendering this approach inapplicable to our blend systems. Furthermore, since neat PEO is highly crystalline, any interlamellar incorporation of the amorphous polymer in the blends is likely to drive w_c into the intermediate range $0.3 < w_c < 0.7$, which once again eliminates the minimum as a viable option. This leaves the remaining alternative: the average long period. While the position of the first correlation maximum yields the average size of the long period for an *ideal* lamellar model, it generally corresponds to its most probable value[35,38] in the pseudo-two phase case. Lorentz peak positions may not be suitable either since these are considered as weight-average values[37] whereas number-average dimensions[34,39] are extracted from the self-correlation triangle, hence the subscript n for average long period and crystal and amorphous thicknesses in the above equations. However, since our systems are isothermally crystallized, minimal distributions in crystal thickness are expected at a constant supercooling. Moreover, since over 70% of the PEO in the blends is crystalline, and blend compositions containing up to only 20−30% diluent are utilized for SAXS analysis, interlamellar amorphous layer distributions are also expected to be relatively narrow. It is reasonable, therefore, to assume a narrow distribution for the long period. Accordingly, the first correlation maximum was used as the input parameter for correlation function analysis.

Optical Microscopy. Development of the spherulitic superstructure was observed under crossed polarizers using an Olympus BH-2 microscope equipped with a Mettler FP82 hot stage which was maintained at the crystallization temperature. Samples were heated at 100 °C for 5 min in another hot stage and rapidly transferred to the hot stage positioned on the microscope stage. The growing spherulites were recorded with the help of a video hookup. Measurements were made at suitable time intervals from the video monitor, taking the curvature of the screen into account. Measured spherulite sizes were scaled to their true values by applying an appropriate conversion factor.

III. Results and Discussion

A. Neat PEO. Table 2 shows average lamellar parameters for neat PEO at $T_c = 45$ and 50 °C calculated from (1) the Lorentz long period and $w_c = \phi_c$ and (2) the correlation function. As expected, the crystal thickness increases as T_c increases. Since $\phi_c > 0.7$ at these crystallization temperatures, the correlation function minimum was additionally used (the baseline is visible) to provide an independent measure of the crystal thickness and linear crystallinity. The results are in good agreement and support our assumption that $w_c = \phi_c$ for neat PEO.

Table 2. SAXS Parameters for Neat PEO

	T_c (°C)	w_c	$\langle L \rangle$ (nm)	$\langle l_a \rangle$ (nm)	$\langle l_c \rangle$ (nm)
Lorentz intensities[b]	45	0.75 ± 0.02[a]	24.3 ± 1.0	6.1 ± 0.5	18.2 ± 0.9
($w_c = \phi_c$)	50	0.77 ± 0.02[a]	27.9 ± 1.3	6.4 ± 0.6	21.5 ± 1.1
correlation function[c]	45	0.69 ± 0.04	24.3 ± 1.1	7.6 ± 1.6	16.7 ± 1.2
($\langle L \rangle$ = first maximum)	50	0.72 ± 0.04	27.2 ± 0.9	7.6 ± 0.9	19.6 ± 1.1
correlation function[c]	45	0.75 ± 0.01	27.8 ± 2.2	6.9 ± 0.4	20.9 ± 2.2
(baseline = minimum)	50	0.77 ± 0.01	31.3 ± 2.8	7.1 ± 0.5	24.2 ± 2.8

[a] Volume fraction bulk crystallinity from DSC. [b] Error in the measured long period is estimated from the breadth of the Lorentz-corrected peak at the apex; errors in $\langle l_a \rangle$ and $\langle l_c \rangle$ are estimated using standard formulas for error propagation.[48] [c] Errors in correlation function parameters are estimated using standard formulas for error propagation; standard deviations in the slope and intercept of the linear fit to the self-correlation portion of the correlation function and the breadth of the first correlation maximum/mimimum (where applicable) are utilized as sources of error.

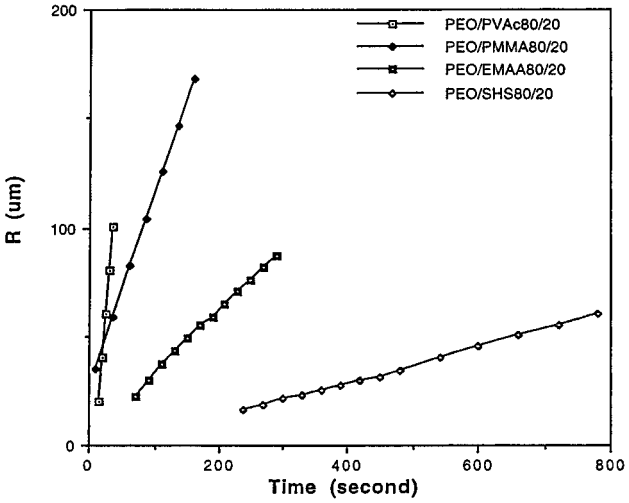

Figure 2. Spherulite radius as a function of time at $T_c = 45$ °C for 80/20 blends: (⊡) PVAc; (◆) PMMA; (□) EMAA55; (◇) SHS50.

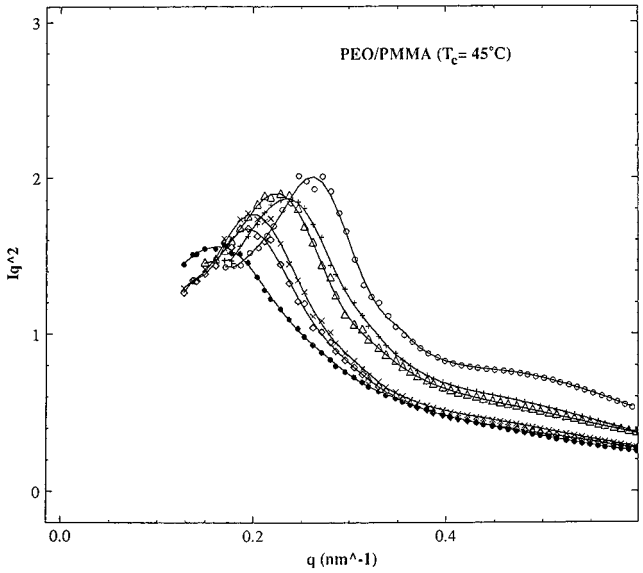

Figure 3. Lorentz-corrected SAXS intensities as a function of scattering vector for PEO and selected PEO/PMMA blends crystallized at 45 °C: (○) 100 PEO/0 PMMA; (+) 90/10; (△) 85/15; (×) 80/20; (◇) 75/25; (●) 70/30.

At each crystallization temperature, the electron density difference was calculated using the correlation function. The two values were averaged, yielding an electron density of 0.614 ± 0.002 mol of electrons/cm^3 for amorphous PEO. This corresponds to a mass density of 1.12 g/cm^3, in agreement with the literature value.[29]

B. Weakly Interacting Blends: PEO/PMMA and PEO/PVAc. Both weakly interacting systems, PEO/PMMA and PEO/PVAc, display linear spherulitic growth over the entire composition range at $T_c = 45$ °C. The lower T_g mixtures, PEO/PVAc, crystallize rapidly at 45 °C (see, for example, Figure 2) while corresponding spherulitic growth rates for PEO/PMMA blends are somewhat lower (by a factor of ∼3−10 at $T_c = 45$ °C, depending on blend composition), as would be expected for a higher T_g diluent. In both cases, volume-filling spherulites are observed at all compositions, indicating that the diluents reside completely within the spherulites. These results are in general agreement with those of other authors.[40−42]

The two weakly interacting blends display strikingly different SAXS behavior when crystallized at 45 °C. Figure 3 presents Lorentz-corrected scattering data for PEO and several PEO/PMMA blends crystallized at 45 °C. The scattering peaks move to lower q, or larger long periods, with increasing PMMA content. For $\chi \sim 0$, it is reasonable to expect the crystal thickness to be independent of blend composition; i.e. $\langle l_c \rangle_{blend} = \langle l_c \rangle_{neat\ PEO}$. As shown in Figure 4, the average long periods calculated for $w_c = \phi_c$ and $\langle l_c \rangle_{blend} = \langle l_c \rangle_{neat\ PEO}$ agree well with the corresponding experimental values, suggesting complete interlamellar incorporation of PMMA at all compositions studied.

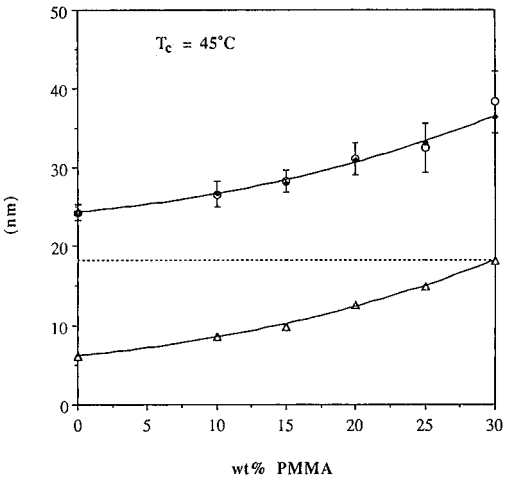

Figure 4. Comparison of experimental long periods with those derived by assuming complete interlamellar incorporation for PEO/PMMA blends: (○) experimental long period; (◆) long period calculated for all-interlamellar incorporation [$\langle l_c \rangle_{neat\ PEO}/\varphi_c$]; (△) amorphous layer thickness for all-interlamellar case [$\langle l_a \rangle_{model} = \langle l_c \rangle_{PEO}(1/\varphi_c - 1)$]; (···) $\langle l_c \rangle_{PEO} = 18.2$ nm.

ϕ_c falls in the range $0.4 < \phi_c < 0.7$ for the PEO/PMMA blends, so that for the case of all-interlamellar PMMA

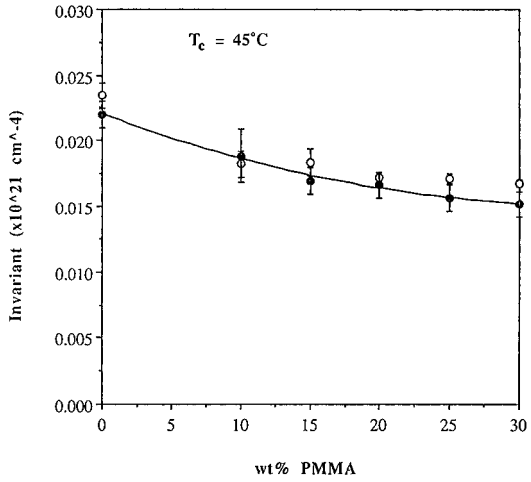

Figure 5. Experimental and calculated invariants for PEO/PMMA blends crystallized at 45 °C: (●) calculated all-interlamellar two-phase invariant; (○) experimental invariant, Q_{fit}, from correlation function. The statistical error in Q_{fit} values in this and subsequent plots is on the order of 2−4%, which is smaller than the size of the symbol used in the plots; errors in Q_{int} arise from an uncertainty of ±0.02 in ϕ_c values.

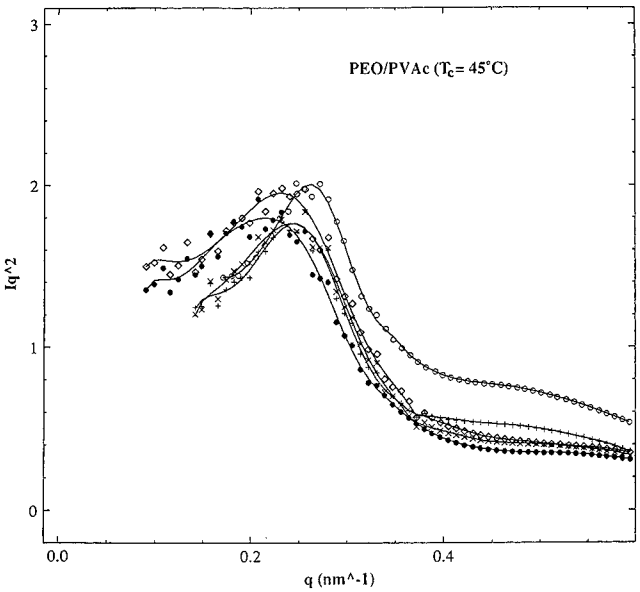

Figure 6. Lorentz-corrected SAXS intensities as a function of scattering vector for PEO and selected PEO/PVAc blends crystallized at 45 °C: (○) 100 PEO/0 PVAc; (+) 90/10; (×) 80/20; (◇) 75/25; (●) 70/30.

placement, $w_c(1 - w_c)$ does not vary appreciably and the invariant is principally sensitive to the bulk electron density difference, $\Delta\eta$. Since the electron density of PMMA lies between those of amorphous and crystalline PEO, increasing incorporation of PMMA in the interlamellar regions would result in a reduction in $\Delta\eta$, which in turn leads to a reduction in the calculated all-interlamellar invariant, as depicted in Figure 5. The excellent agreement between the experimental and calculated values lends further credence to the conclusion that PMMA resides completely within interlamellar regions, within experimental uncertainty. Similar results have been reported previously by Russell and coworkers.[6]

In the case of PEO/PVAc blends, the scattering peaks broaden somewhat with increasing PVAc content but the maxima shift only slightly to lower q values (Figure 6). Experimental and calculated (all-interlamellar PVAc placement) invariants are presented in Figure 7. The

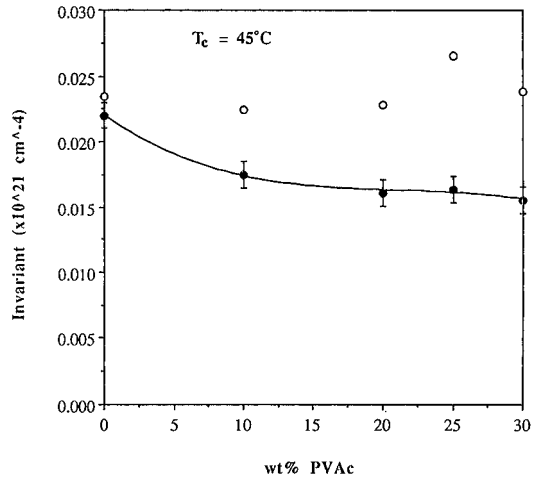

Figure 7. Experimental and calculated invariants for PEO/PVAc blends crystallized at 45 °C: (●) calculated all-interlamellar two-phase invariant; (○) experimental invariant, Q_{fit}, from the correlation function.

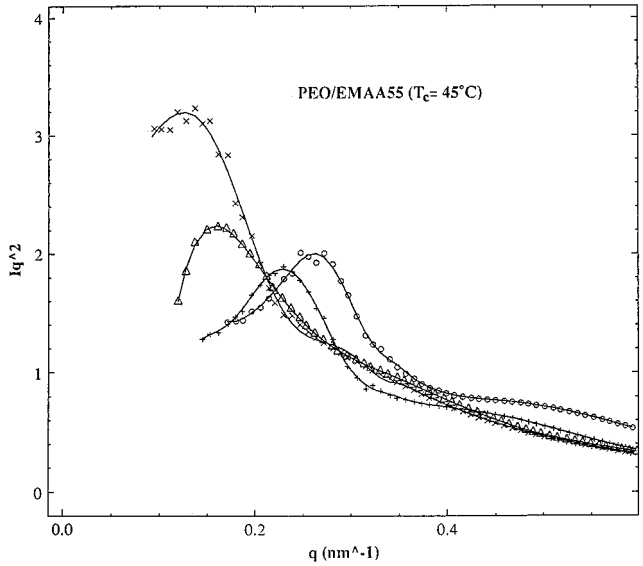

Figure 8. Lorentz-corrected SAXS intensities as a function of scattering vector for PEO and selected PEO/EMAA55 blends crystallized at 45 °C: (○) 100 PEO/0 EMAA55; (+) 90/10; (△) 85/15; (×) 80/20.

plots are drawn to the same scale and over the same composition range as the PEO/PMMA blends in order to facilitate comparison between the behavior of these systems. Both PVAc and PMMA have comparable electron densities and the bulk crystallinities of all PEO/PVAc and PEO/PMMA blends lie in the intermediate range. As such, their calculated all-interlamellar invariants exhibit very similar trends. However, the experimental Q_{fit} for the PEO/PVAc blends do not change appreciably with increasing PVAc content, in contrast with those for PEO/PMMA. These findings, in conjuction with results of the optical microscopy experiments, suggest at least partial exclusion of PVAc from the interlamellar to the interfibrillar region during crystallization at 45 °C. Unfortunately, quantitative determination of the extent of PVAc migration was not possible due to the low electron density contrast between amorphous PEO and PVAc.

C. Strongly Interacting Blends: PEO/EMAA55 and PEO/SHS50. Lorentz-corrected SAXS intensities vs q for PEO/EMAA55 blends are presented in Figure 8. A dramatic increase in long period is observed as

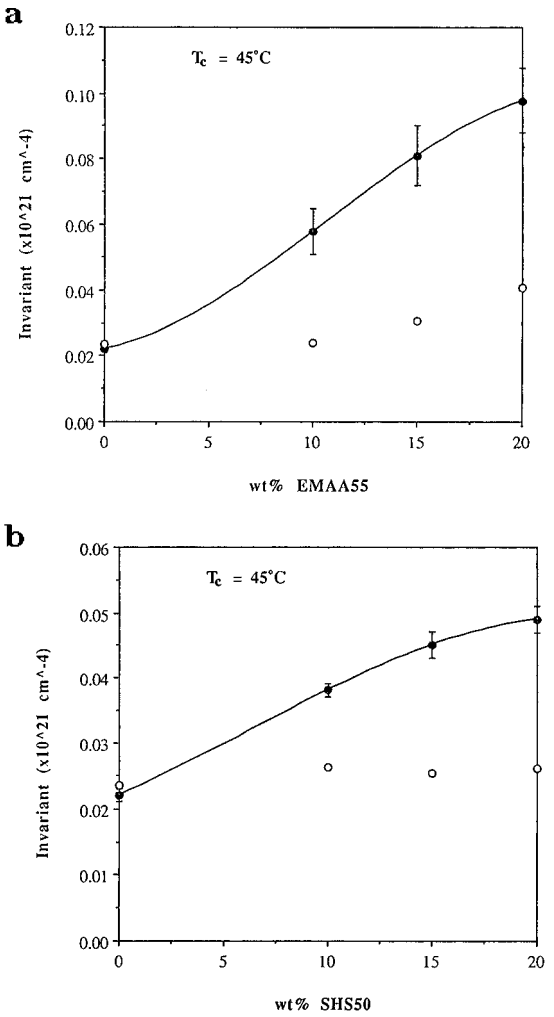

Figure 9. Experimental and calculated invariants for (a) PEO/EMAA55 and (b) PEO/SHS50 blends crystallized at 45 °C: (●) calculated all-interlamellar two-phase invariant; (○) experimental invariant, Q_{fit}, from correlation function.

EMAA55 content is increased up to only 20%. One may at first take this as evidence that the EMAA55 is located in interlamellar regions but comparison of the expected SAXS invariant for the case of all-interlamellar incorporation vs that measured experimentally leads to a quite different conclusion (Figure 9a). EMAA55 has an electron density that is substantially smaller than those of neat amorphous and crystalline PEO, and even modest interlamellar inclusion of the amorphous polymer would be expected to lead to a significant change in the invariant for PEO/EMAA55 blends, as depicted by the solid line in Figure 9a. Thus these data strongly suggest significant displacement of EMAA55 to extralamellar regions. Microstructural parameters extracted from the correlation function analysis of the PEO/EMAA55 blends are presented in Figure 10. The results clearly show that the increase in long period with increasing diluent content is primarily due to an increase in lamellar thickness, which is consistent with a lower degree of supercooling (i.e. a significant equilibrium melting point depression), as expected for strongly interacting mixtures.

The same conclusion arises from a consideration of invariants (see Figure 9b) and Lorentz-corrected intensities (Figure 11) for the PEO/SHS50 blends: PEO/SHS50 blends containing up to 20% diluent display a systematic increase in long period with increasing SHS50 content but the experimental invariants suggest

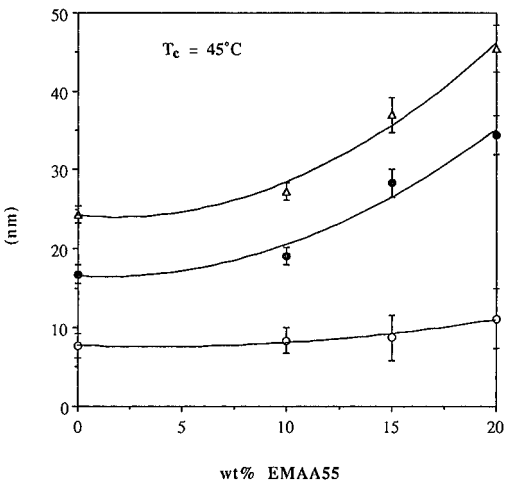

Figure 10. Microstructural parameters via correlation function analysis for PEO/EMAA55 blends crystallized at 45 °C: (△) average long period from position of first correlation maximum; (●) average crystal thickness; (○) average amorphous layer thickness.

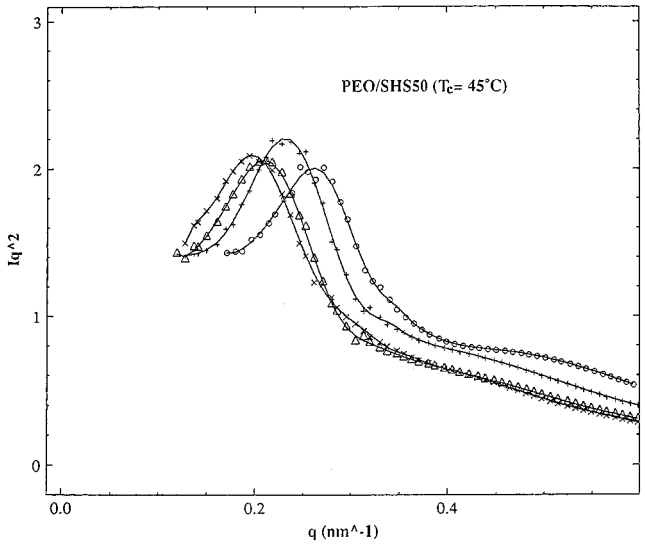

Figure 11. Lorentz-corrected SAXS intensities as a function of scattering vector for PEO and selected PEO/SHS50 blends crystallized at 45 °C: (○) 100 PEO/0 SHS50; (+) 90/10; (△) 85/15; (×) 80/20.

substantial exclusion of the diluent from the interlamellar regions. Again, correlation function analysis (Figure 12) indicates thicker lamellae as the cause of the increase in long period. Unlike the PEO/EMAA55 system, however, the increases in crystal thickness are more modest, suggesting that the equilibrium melting point depression is not as pronounced for this system.

From the kinetic theory of crystallization[43]

$$l_c = \beta l_g^* = \beta[2\sigma_e T_m^\circ/\Delta H_f^\circ \Delta T] \qquad (9)$$

where l_g^* is the initial crystal thickness, β the factor by which the crystals thicken at T_c, and σ_e the end surface free energy. If we assume, to a first approximation, that β and σ_e are independent of blending and recognize that changes in T_m° (in kelvin units) have only a small effect on l_c in eq 9, then we can write. $l_c = z(1/\Delta T)$, where z is then a constant for PEO and the blends. This then permits us to estimate the degree of supercooling at which our EMAA55 and SHS50 blends were crystallized by comparing the experimental crystal thicknesses with those determined by Arlie *et al.* for neat PEO.[44] This

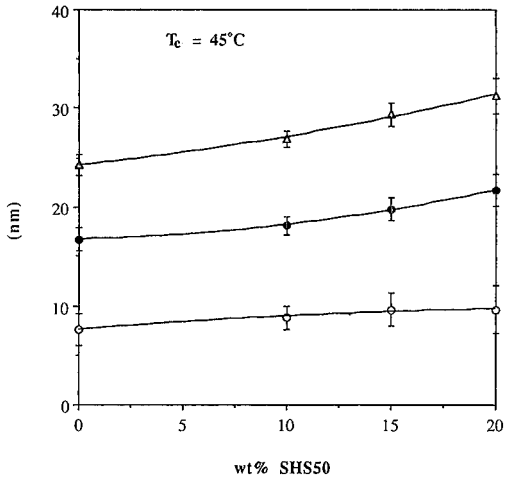

Figure 12. Microstructural parameters via correlation function analysis for PEO/SHS50 blends crystallized at 45 °C: (△) average long period from position of first correlation maximum; (●) average crystal thickness; (○) average amorphous layer thickness.

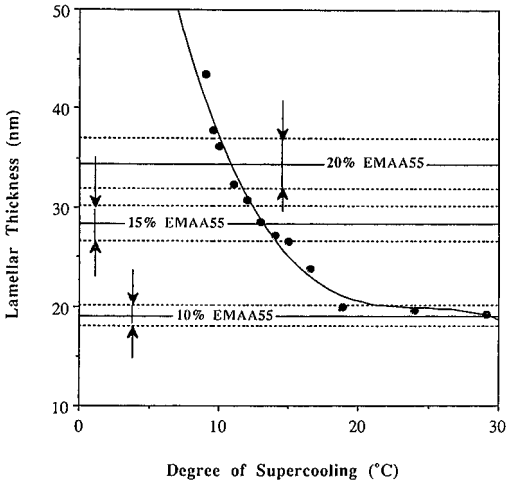

Figure 13. Comparison of SAXS crystal thicknesses reported by Arlie *et al.*[44] as a function of degree of supercooling (using $T_m° = 69$ °C[28]) with those determined experimentally for PEO/EMAA55 blends: (●) data from Arlie *et al.*;[44] the horizontal solid lines represent the average lamellar thicknesses for three EMAA55 blends and the dashed lines the uncertainty in the measured value.

is illustrated in Figures 13 and 14. The solid horizontal lines represent the lamellar thicknesses, l_c, derived from correlation function analysis. The broken lines flanking each l_c denote the uncertainty in the measured values. The experimental data of Arlie and co-workers is represented by filled circles and is fit by a solid line. The degree of supercooling at a given blend composition is given by the intersection of the horizontal lines (or $l_c \pm$ error) pertaining to that composition with the fit to Arlie *et al.*'s data. It therefore appears from Figure 13 that the addition of EMAA55 to PEO can effectively depress the supercooling by as much as ca. 9−14 °C in the range of 15−20% EMAA55. A depression of 2−5 °C in the equilibrium melting point ($T_m°$) has been reported previously for PEO/EMAA55 blends containing up to 30% EMAA55.[45] Although the absolute value of the reported depression is somewhat uncertain,[42,46] our results suggest a much greater reduction in the degree of supercooling for 80/20 PEO/EMAA55 crystallized at 45 °C. The behavior of the SHS50 blends (Figure 14) is similar although the changes in crystal thickness with SHS50 composition are not as large as for PEO/

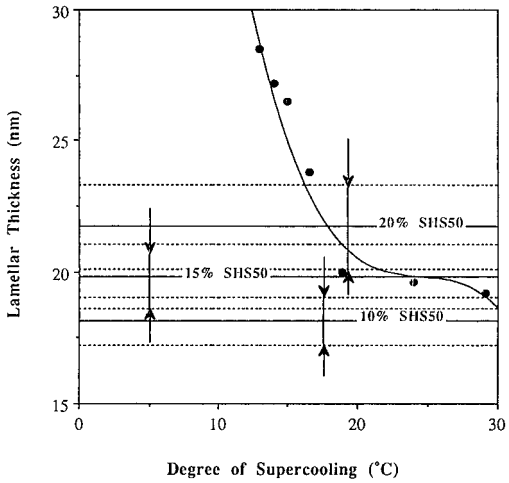

Figure 14. Comparison of SAXS crystal thicknesses reported by Arlie *et al.*[44] as a function of degree of supercooling (using $T_m° = 69$ °C[28]) with those determined experimentally for PEO/SHS50 blends: (●) data from Arlie *et al.*;[44] the horizontal solid lines represent the average lamellar thicknesses for three SHS50 blends and the dashed lines the uncertainty in the measured value.

EMAA55, suggesting that the melting point depression is not as large for this blend (but still very significant; ca. 6 °C for the blend containing 20% SHS50).

Crystallization rates for these systems are much lower than those for their weakly interacting counterparts. For example, since PVAc and EMAA55 have similar glass transition temperatures, their blends with PEO might initially be expected, to a first approximation, to crystallize at comparable rates. However, PEO/EMAA55 crystallizes much more slowly than PEO/PVAc: at 20% EMAA55 concentration, the spherulitic growth rate (G) is an order of magnitude lower than that of the 80/20 PEO/PVAc blend (see Figure 2). At 30% EMAA55 concentration, the growth rate not only diminishes further ($G = 0.37$ μm/min for the 70/30 EMAA blend compared to 150 μm/min for the corresponding PVAc mixture) but growth ceases before the spherulites impinge. On cooling to room temperature, the spherulites resume growing, eventually becoming volume-filling. Such behavior is characteristic of a decrease in the degree of supercooling (ΔT) brought about by the addition of a strongly interacting diluent.

PEO/SHS50 blends are found to crystallize at even slower rates than the corresponding PEO/EMAA55 blends (e.g. a factor of 3 slower at 70/30). The 70/30 PEO/SHS50 blend crystallizes at 45 °C much like the 70/30 EMAA55 blend. However, growth does not resume on cooling to room temperature, implying significant buildup of the high-T_g SHS50 at the spherulitic boundaries. Since the addition of a high-T_g diluent in itself serves to retard the crystal growth rate by raising the T_g of the blend, the crystallization behavior of the 70/30 PEO/SHS50 blend can be attributed to the combination of a lower degree of supercooling and the substantially higher glass transition temperature of SHS50 relative to the T_g of PEO.

Both PEO/EMAA55 and PEO/SHS50 blends exhibit volume-filling spherulites up to a diluent concentration of about 20 wt %. These observations, in concert with SAXS results, indicate partial exclusion of the diluent into interfibrillar regions at these compositions. The distribution of the diluent between the interlamellar and interfibrillar regions can be estimated using the measured bulk crystallinities and correlation function

Table 3. Amorphous PEO and Diluent Distribution in PEO/EMAA55 and PEO/SHS50 Blends[a]

blend	wt % diluent	v_s	η_l	ϕ_a	IL_a	IF_a	ϕ_d	IL_d	IF_d	G (μm/min)
PEO/EMAA55	10	≈1	0.613 ± 0.002	0.19 ± 0.02	–	–	0.12 ± 0.02	–	–[b]	134
	15	0.90 ± 0.04	0.595 ± 0.003	0.12 ± 0.02	0.16 ± 0.02	≈0	0.19 ± 0.02	0.09 ± 0.04	0.10 ± 0.04	–
	20	0.83 ± 0.03	0.581 ± 0.004	0.12 ± 0.02	0.12 ± 0.01	≈0	0.25 ± 0.02	0.08 ± 0.01	0.17 ± 0.03	22.4
PEO/SHS50	10	0.95 ± 0.05 (≈1)	0.610 ± 0.003	0.25 ± 0.02	–	–	0.11 ± 0.02	–	–[b]	26.4
	15	0.90 ± 0.05	0.610 ± 0.003	0.23 ± 0.02	0.27 ± 0.04	≈0	0.17 ± 0.02	0.07 ± 0.05	0.10 ± 0.05	–
	20	0.78 ± 0.04	0.601 ± 0.003	0.24 ± 0.02	0.16 ± 0.03	0.08 ± 0.04	0.22 ± 0.02	0.08 ± 0.02	0.14 ± 0.03	2.28

[a] v_s = volume fraction of lamellar stacks = ϕ_c/w_c; η_l = average electron density of interlamellar regions (from eq 4); IL_a = amorphous PEO in interlamellar regions = $\phi_{la}(1 - w_c)v_s$, where $\phi_{la} = (\eta_l - \eta_d)/(\eta_a - \eta_d)$ ($\eta_a = 0.614 \pm 0.002$ mol of electrons/cm^3); IF_a = amorphous PEO in interfibrillar regions = $\phi_a - IL_a$; IF_d = diluent in interfibrillar regions = $1 - v_s = IF_a$; IL_d = diluent in interlamellar regions = $\phi_d - IF_d$; G = spherulitic growth rate (from optical microscopy). [b] Value uncertain (see text).

parameters, as shown in Table 3. Definitions and computational details of the various parameters are listed in the legend in Table 3. Corresponding spherulitic growth rates are also provided. Errors in the calculated values have been determined using standard error propagation formulas.[48] Since the overall volume fractions of crystalline PEO (ϕ_c), amorphous PEO (ϕ_a), and diluent polymer (ϕ_d) are obtained from DSC bulk crystallinities, the same uncertainty is applied to all three volume fractions.

At 10% diluent content, the bulk and linear crystallinities are comparable within experimental error; as such, it is difficult to quantitatively ascertain diluent distribution between the interlamellar and interfibrillar regions. However, comparison of the experimental and calculated invariants (see Figure 9) does indicate some exclusion from the interlamellar regions. As diluent content is increased to 20%, both systems exhibit a corresponding increase in the fraction of interfibrillar material, $1 - v_s$, and a significant reduction in spherulitic growth rate. Moreover, up to 20% diluent content (15% for PEO/SHS50), almost all of the amorphous PEO resides in interlamellar regions; i.e., $IF_a \approx 0$. Therefore, the interfibrillar regions are comprised mainly of the diluent polymer at these compositions. However, ~30% (by volume) of the amorphous PEO is included in the interfibrillar regions for the 20% SHS50 blend, yielding a value for the interfibrillar T_g (using the Fox–Flory equation and PEO $T_g \sim -55$ °C[23]) near the crystallization temperature. This is precisely what would be expected in systems containing a relatively high-T_g diluent: diffusion of the crystallizable polymer to crystal growth fronts will effectively cease when T_g of the mixed phase approaches T_c.

IV. Summary

A number of inferences can be drawn from the above analysis. The contrasting behavior of the two weakly interacting systems seems to suggest that the mobility of the amorphous component at T_c decides diluent location: relatively high-T_g PMMA is trapped between crystal lamellae whereas low-T_g PVAc can diffuse away from the crystal growth front and reside at least partially in interfibrillar regions. However, an examination of the microstructures of the two high-T_g systems, PEO/PMMA and PEO/SHS50, clearly demonstrates that diluent mobility is not the sole criterion for amorphous phase segregation. Although SHS50 has a significantly higher T_g (and molecular weight) and therefore reduced mobility in the mixed environment compared to PMMA, SHS50 is found to reside in interfibrillar regions up to a blend composition of 20%, becoming at least partially interspherulitic at higher concentrations, whereas PMMA is completely interlamellar at all blend compositions studied. The appreciably lower crystal growth rates for the PEO/SHS50 blends allow more time for SHS50 diffusion over larger distances from the growth front. Similar behavior would also be expected for PEO/PMMA blends, at sufficiently high crystallization temperatures. Such a relationship between the scale of diluent segregation and relative diffusion and growth rates has been proposed previously by Keith and Padden.[18,47]

A comparison of the two low-T_g systems, PEO/PVAc and PEO/EMAA55, further illustrates the effect of crystallization rate on diluent migration. The diluent is extralamellar in both cases but diffuses over larger distances for the more slowly crystallizing PEO/EMAA55 blends, becoming partly interspherulitic at ~30% EMAA55 content. In the case of the more rapidly crystallizing PEO/PVAc blends, diluent segregation is limited to the interfibrillar region even up to 40% PVAc content. Despite the lower molecular weight of EMAA55 compared to PVAc, the fact that the amorphous polymers in both slow-crystallizing systems (PEO/EMAA55 and PEO/SHS50) exhibit a similar degree of segregation with increasing diluent content, irrespective of relative diluent T_gs and molecular weights, strongly favors crystal growth rate as a crucial factor in the extent of migration of the amorphous component. Moreover, since the low crystal growth rates observed in both strongly interacting systems, PEO/EMAA55 and PEO/SHS50, are principally due to a lower degree of supercooling, we conclude that the presence of strong intermolecular interactions helps to promote amorphous phase segregation by depressing the crystal growth rate.

For the systems investigated, it follows, therefore, that while the effect of diluent mobility cannot be ignored, it is the growth rate of the PEO crystals, and hence the factors that influence the growth rate, which dominate the length scale of diluent segregation at the crystallization temperature explored in our study.

Acknowledgment. This research was supported in part by the Division of Materials Science, U.S. Department of Energy, under Contract No. DE-AC05-84OR21400 with Martin Marietta Energy Systems, Inc. We would also like to acknowledge the donors of the Petroleum Research Fund, administered by the American Chemical Society, for support of this work. In addition, we would like to express our thanks to Prof. Sanat Kumar for a number of helpful discussions throughout the course of this work and Stephen Henning and Jennifer Woodring for assisting with initial crystal growth experiments.

References and Notes

(1) Russell, T. P.; Stein, R. S. *J. Polym. Sci., Polym. Phys. Ed.* **1983**, *21*, 999.

(2) Morra, B. S.; Stein, R. S. *Polym. Eng. Sci.* **1984**, *24*, 311.
(3) Briber, R. M.; Khoury, F. *Polymer* **1987**, *28*, 38.
(4) Hahn, B.; Hermann-Schonherr, O.; Wendorff, J. *Polymer* **1987**, *28*, 201.
(5) Silvestre, C.; Karasz, F. E.; MacKnight, W. J.; Martuscelli, E. *Eur. Polym. J.* **1987**, *23*, 745.
(6) Russell, T. P.; Ito, H.; Wignall, G. D. *Macromolecules* **1988**, *21*, 1703.
(7) Defieuw, G.; Groeninckx, G.; Reynaers, H. *Polym. Commun.* **1989**, *30*, 267.
(8) Defieuw, G.; Groeninckx, G.; Reynaers, H. *Polymer* **1989**, *30*, 595.
(9) Crevecoeur, G.; Groeninckx, G. *Macromolecules* **1991**, *24*, 1190.
(10) Lohse, D. J.; Wissler, G. E. *J. Mater. Sci.* **1991**, *26*, 743.
(11) Zemel, I. S.; Roland, C. M. *Polymer* **1992**, *33*, 3427.
(12) Runt, J. P.; Zhang, X.; Miley, D. M.; Gallagher, K. P.; Zhang, A. *Macromolecules* **1992**, *25*, 3902.
(13) Saito, H.; Stuhn, B. *Macromolecules* **1994**, *27*, 216.
(14) Yoon, D. Y.; Ando, Y.; Rozstaczer, S.; Kumar, S. K.; Alfonso, G. C. *Macromol. Chem., Macromol. Symp.* **1991**, *50*, 183.
(15) Hudson, S. D.; Davis, D. D.; Lovinger, A. J. *Macromolecules* **1992**, *25*, 1759.
(16) Huo, P. P.; Cebe, P.; Capel, M. *Macromolecules* **1993**, *26*, 4275.
(17) Sauer, B. B.; Hsiao, B. S. *J. Polym. Sci., Polym. Phys. Ed.* **1993**, *31*, 901.
(18) Keith, H. D.; Padden, F. J. *J. Polym. Sci., Polym. Phys. Ed.* **1987**, *25*, 229.
(19) Silvestre, C.; Cimmino, S.; Martuscelli, E.; Karasz, F.; MacKnight, W. J. *Polymer* **1987**, *28*, 1190.
(20) Privalko, V. P.; Petrenko, K. D.; Lipatov, Y. S. *Polymer* **1990**, *31*, 1277.
(21) Ito, H.; Russell, T. P.; Wignall, G. D. *Macromolecules* **1987**, *20*, 2213.
(22) Coleman, M. M.; Graf, J. F.; Painter, P. C. *Specific Interactions and the Miscibility of Polymer Blends*; Technomic Press: Lancaster, PA, 1991.
(23) Talibuddin, S.; Runt, J. *Polymer*, submitted for publication.
(24) Coleman, M. M.; Lee, J. Y.; Serman, C. J.; Wang, Z.; Painter, P. C. *Polymer* **1989**, *30*, 1298.
(25) Moskala, E. J.; Varnell, D. F.; Coleman, M. M. *Polymer* **1985**, *26*, 228.
(26) Ting, S. P.; Bulkin, B. J.; Pearce, E. M. *J. Polym. Sci., Polym. Phys. Ed.* **1981**, *19*, 1451.
(27) Lee, J. Y.; Painter, P. C.; Coleman, M. M. *Macromolecules* **1988**, *21*, 346.
(28) Wunderlich, B. *Macromolecular Physics*; Academic Press: New York, 1980; Vol. 3.
(29) *Polymer Handbook*, 3rd ed.; Brandrup, J., Immergut, E. H., Eds.; Wiley: New York, 1989.
(30) Wignall, G. D.; Lin, J. S.; Spooner, S. *J. Appl. Crystallogr.* **1990**, *23*, 241.
(31) Russell, T. P.; Lin, J. S.; Spooner, S.; Wignall, G. D. *J. Appl. Crystallogr.* **1988**, *21*, 629.
(32) Ruland, W. *J. Appl. Crystallogr.* **1971**, *4*, 70.
(33) Bonart, R.; Müller, E. H. *J. Macromol. Sci., Phys.* **1974**, *B10*, 177.
(34) Strobl, G. R.; Schneider, M.; Voigt-Martin, I. *J. Polym. Sci., Polym. Phys. Ed.* **1980**, *19*, 1361.
(35) Strobl, G. R.; Schneider, M. *J. Polym. Sci., Polym. Phys. Ed.* **1980**, *18*, 1343.
(36) Elsner, G.; Koch, M. H. J.; Bordas, J.; Zachmann, H. G. *Makromol. Chem.* **1981**, *182*, 1263.
(37) Vonk, C. G. *J. Appl. Crystallogr.* **1978**, *11*, 541.
(38) Crist, B.; Morosoff, N. *J. Polym. Sci.* **1973**, *11*, 1023.
(39) Baltá Calleja, E.; Vonk, C. G. *X-ray Scattering of Synthetic Polymers*; Elsevier: Amsterdam, 1989.
(40) Martuscelli, E.; Silvestre, C.; Gismondi, C. *Makromol. Chem.* **1985**, *186*, 2161.
(41) Martuscelli, E.; Silvestre, C.; Addonizio, M. L.; Amelino, L. *Makromol. Chem.* **1986**, *187*, 1557.
(42) Alfonso, G. C.; Russell, T. P. *Macromolecules* **1986**, *19*, 1143.
(43) Hoffman, J. D.; Davis, G. T.; Lauritzen, J. I. In *Treatise in Solid State Chemistry*; Hannay, H. B., Ed.; Plenum Press: New York, 1975; Vol. 3.
(44) Arlie, J. P.; Spegt, P.; Skoulios, A. *Makromol. Chem.* **1967**, *104*, 212.
(45) Painter, P. C.; Shenoy, S. L.; Bhagwagar, D. E.; Fishburn, J.; Coleman, M. M. *Macromolecules* **1991**, *24*, 5623.
(46) Runt, J.; Gallagher, K. P. *Polym. Commun.* **1991**, *32*, 180.
(47) Keith, H. D.; Padden, F. J. *J. Appl. Phys.* **1963**, *34*, 2409.
(48) Neter, J.; Wasserman, W. *Applied Linear Statistical Models*, Richard D. Irwin, Inc.: Homewood, IL, 1974.

MA960508F